NANO LETTERS

pubs.acs.org/NanoLett Letter

High-Entropy Polymer Electrolytes Derived from Multivalent Polymeric Ligands for Solid-State Lithium Metal Batteries with Accelerated Li^+ Transport

Fangmin Ye,*,○ Zhixin Wang,○ Mengcheng Li,○ Jing Zhang, Dong Wang, Meinan Liu, Aiping Liu,* Hongzhen Lin, Hee-Tak Kim,* and Jian Wang*

Cite This: *Nano Lett.* 2024, 24, 6850−6857 Read Online

ACCESS | Metrics & More | Article Recommendations | Supporting Information

ABSTRACT: Solid-state polymer-based electrolytes (SSPEs) exhibit great possibilities in realizing high-energy-density solid-state lithium metal batteries (SSLMBs). However, current SSPEs suffer from low ionic conductivity and unsatisfactory interfacial compatibility with metallic Li because of the high crystallinity of polymers and sluggish Li^+ movement in SSPEs. Herein, differing from common strategies of copolymerization, a new strategy of constructing a high-entropy SSPE from multivariant polymeric ligands is proposed. As a protocol, poly(vinylidene fluoride-*co*-hexafluoropropylene) (PH) chains are grafted to the demoed polyethylene imine (PEI) with abundant $-NH_2$ groups via a click-like reaction (HE-PEIgPHE). Compared to a PH-based SSPE, our HE-PEIgPHE shows a higher modulus (6.75 vs 5.18 MPa), a higher ionic conductivity (2.14×10^{-4} vs 1.03×10^{-4} S cm^{-1}), and a higher Li^+ transference number (0.55 vs 0.42). A Li|HE-PEIgPHE|Li cell exhibits a long lifetime (1500 h), and a Li|HE-PEIgPHE|$LiFePO_4$ cell delivers an initial capacity of 160 mAh g^{-1} and a capacity retention of 98.7%, demonstrating the potential of our HE-PEIgPHE for the SSLMBs.

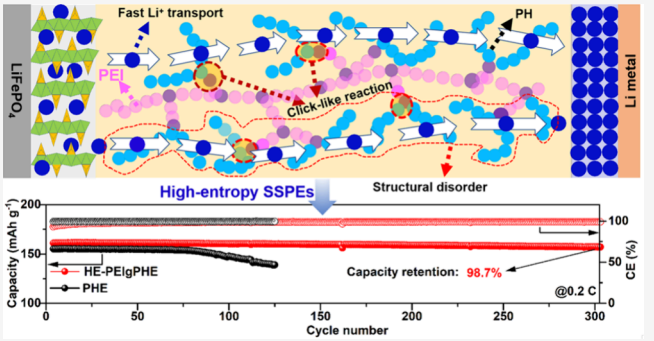

KEYWORDS: *Solid polymer electrolyte, Li metal batteries, high-entropy polymer, polymeric ligand, Li^+ transport*

With the widespread popularization of electric vehicles and portable electronics, there is an urgent increase in demand for high-energy-density storage systems.[1−3] Rechargeable Li-ion batteries (LIBs) have dominated in various fields and largely changed the modern lifestyle.[4−8] In comparison to a conventional graphite anode reaching the capacity bottleneck (372 mAh g^{-1}), a Li metal anode alternatively shows a high theoretical specific capacity (3860 mAh g^{-1}) and an extremely low potential (−3.04 V vs standard hydrogen electrode), which can be used to develop higher energy density Li metal batteries (LMBs).[9−13] However, current LMBs based on the widely-used liquid organic electrolytes show high flammability and severe safety hazards due to the formation of Li dendrites, which retards their practical applications.[14−16] Solid-state polymer electrolytes (SSPEs) featuring high fire retardancy, high flexibility, and high interface compatibility with electrodes are believed to be feasible options to boost the practical use of LMBs.[17,18] In particular, organic-solvent-free SSPEs consisting of Li salts and polymer-based solid substrates[19] show great capability in inhibiting the formation/growth of Li dendrites, improving safety and providing high compatibility with high-voltage cathodes.[20] Further, endowing various Li salts with SSPEs leads to some unexpected functionalization.[21−25] Despite the advantages, their low thermal stability, weak mechanical strength,[26] and low ionic conductivity[27,28] remain a critical challenge, discouraging the development of practical solid-state LMBs (SSLMBs).[29,30]

To solve the aforementioned problems, three effective strategies have been presented in recent years: (i) incorporating inorganic particles such as $Li_xLa_yZr_zTa_mO_n$ (LLZTO) and $Li_xAl_yGe_z(PO4)_m$ (LAGP) into SSPEs to realize more Li^+ coordination sites and thus increase the ionic conductivity;[31,32] (ii) introducing ionic liquids to form gel electrolytes to better wet the interface between the SSPE and metallic Li;[33,34] (iii) cross-linking or copolymerization decreasing the crystallinity of polymers and enhancing Li^+ conductivity and mechanical properties of SSPEs.[35,36] However, the above approaches do not fully address the trade-off among mechanical properties, interfacial stability, and ionic conductivity, which is one of the deep-rooted problems in SSPE research.

Received: January 11, 2024
Revised: May 5, 2024
Accepted: May 7, 2024
Published: May 9, 2024

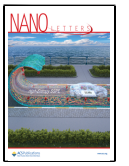

https://doi.org/10.1021/acs.nanolett.4c00154
Nano Lett. 2024, 24, 6850−6857

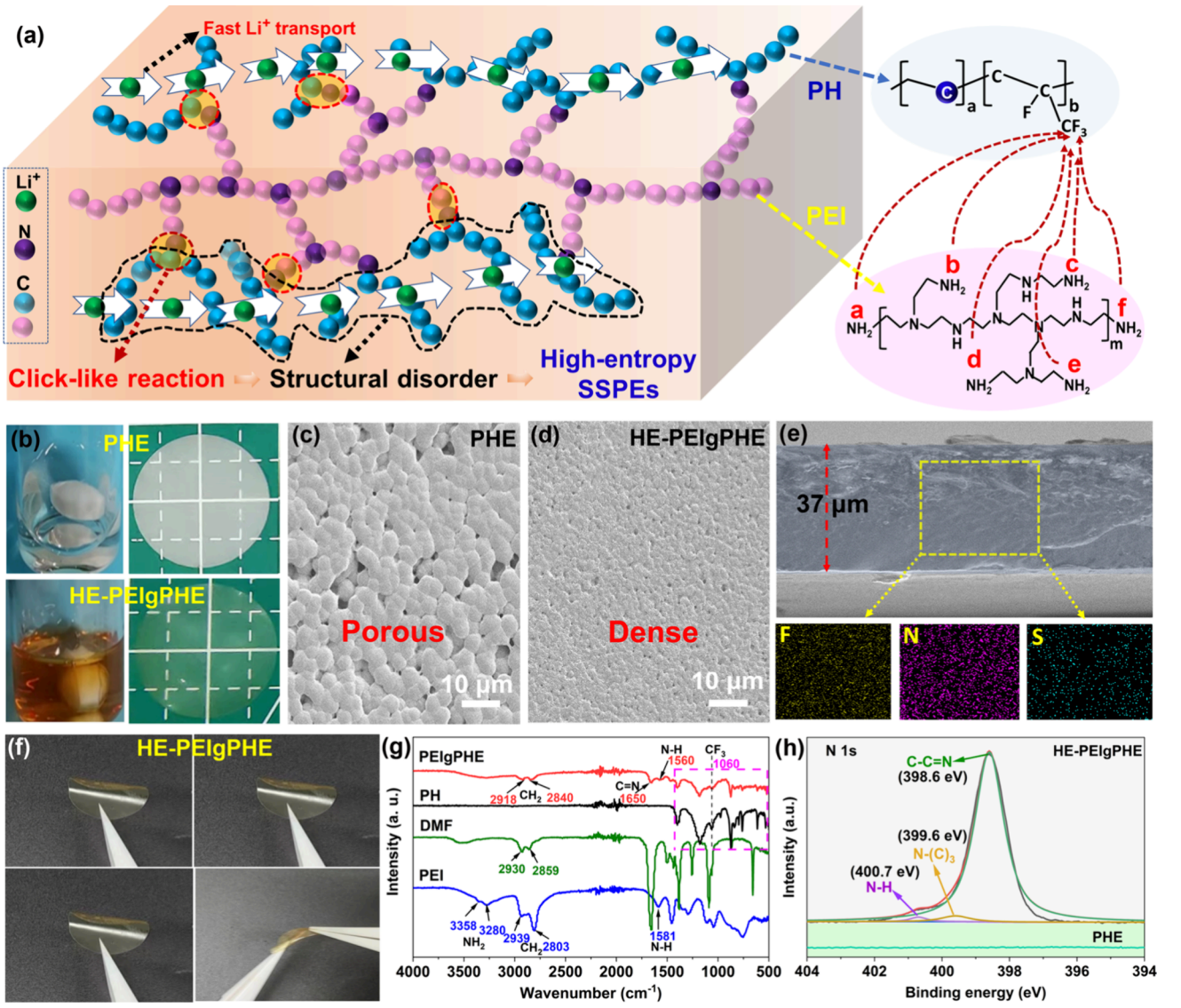

Figure 1. The concept of high-entropy SSPE and the physical characteristics of PHE and HE-PEIgPH. (a) Concept of a high-entropy SSPE based on the click-like reaction of PH and PEI. (b) Digital photographs of PHE and HE-PEIgPHE slurries and membranes. Surface SEM images of (c) PHE and (d) HE-PEIgPHE. (e) Cross-sectional SEM image and elementary mapping images (F, N, and S) for HE-PEIgPHE. (f) Digital photos of the HE-PEIgPHE membrane under bending, folding, and twisting. (g) Comparison of FT-IR spectra of DMF, PEI, PHE, and HE-PEIgPH. (h) XPS spectrum of N 1s for PHE and HE-PEIgPHE, respectively.

In the development of conventional SSPEs, various polymer matrixes, such as poly(ethylene oxide) (PEO), poly(methyl methacrylate) (PMMA), poly(vinylidene fluoride-hexafluoropropylene) (PH), and polyacrylonitrile (PAN), have been presented. Among them, the fluorine-rich PH as a matrix shows a strong electrical adsorption, high stability in high-voltage cathodes, and a low glass transition temperature of 90 °C; therefore, PH-based SSPEs have attracted more and more attention. In addition, the enthalpy of a multicomponent system has been a major design parameter; the intermolecular interactions among ions, polymer segments, and additives are regulated to control the properties. Deviating from the paradigm, a brand-new design concept of high-entropy polymers was recently suggested. By increasing the degree of disorder in a multicomponent SSPE, mechanical and ionic conducting properties can be concurrently improved. This unique characteristic can be grounded on the entropic effect of reducing ion clustering and increasing entropic elasticity.[37−39] Su et al. reported a high-entropy SSPE that is obtained by introducing newly designed multifunctional ABC miktoarm star terpolymers into poly(ethylene oxide), improving the Li^+ transference number and toughness, and inducing stable Li plating/stripping.[37] However, the need for a suitable solvent required for dissolving various mixed polymers will increase the fabrication difficulty of this class of high-entropy SSPEs. Therefore, to advance high-entropy SSPEs, it is imperative to explore novel, straightforward, and efficient methods for making high-entropy polymeric structures.

Herein, we present a high-entropy SSPE that is achieved by adding a multivariant polymer ligand to a conventional polymer electrolyte. The grafting of polymer chains to the polymer ligands can form a disordered structure for facial Li^+ transport in addition to improve mechanical properties, as illustrated in Figure 1a. To demonstrate our concept, the polyethylene imine (PEI) with abundant NH_2 groups is introduced to a conventional SSPE composed of PH and

https://doi.org/10.1021/acs.nanolett.4c00154
Nano Lett. 2024, 24, 6850−6857

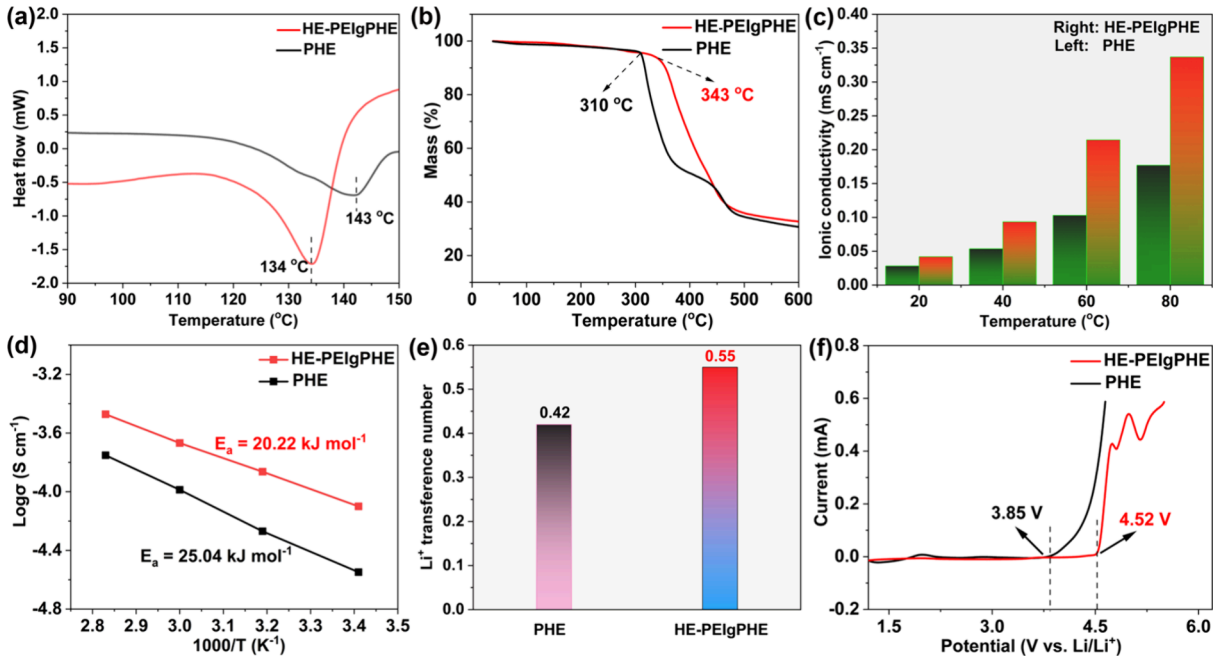

Figure 2. Thermal and electrochemical properties of PHE and HE-PEIgPHE. (a) DSC curves, (b) TGA curves, (c) ionic conductivities at different temperatures, (d) Arrhenius plots, (e) Li^+ transference numbers, and (f) LSV curves tested at a scanning rate of 0.05 mV s^{-1} at 60 °C.

bistrifluoromethanesulfonimide lithium salt (LiTFSI) via a click-like reaction: $RNH_2 + CF_3R' \rightarrow RN{=}CFR' + 2HF$. The abundant grafting sites distributed along the PEI ligands lead to significant disorder of the grafted PH chains, which enhances Li^+ transport, prevents the formation of a Li^+ cluster, and improves the mechanical properties. Impressively, the ionic conductivity and Li^+ transference number of our HE-PEIgPHE were increased with the addition of the multivariant polymeric ligand, delivering values of 2.14×10^{-4} S cm^{-1} and 0.55, respectively. The fabricated Li|HE-PEIgPHE|Li symmetric cell exhibits a long lifetime of over 1500 h with a low overpotential of 30 mV at 0.1 mA cm^{-2}, and the Li|HE-PEIgPHE|$LiFePO_4$ full cell delivers a capacity of 160 mAh g^{-1} at 0.2 C and a high capacity retention of 98.7% within 300 cycles. These results obtained with HE-PEIgPHE demonstrate the efficacy of a high-entropy SSPE in boosting the performance of SSLMBs.

To improve the ionic conductivity and mechanical property of SSPEs, a novel high-entropy SSPE is constructed by grafting polymer chains (branches) on a multivariant polymeric ligand via chemical "click-like" reactions. The grafting leads to disordering of the network structure, providing free volume and channels for Li^+ transport and high mechanical strength. As a proof of concept, PH was used as a branch polymer, and PEI with abundant NH_2 groups was chosen as polymeric ligands (Figure 1a). As depicted at the right in Figure 1a, the rich NH_2(a–f) groups on the PEI can react with $-CF_3$ groups on PH, which leads to topological and disordered structure entropy and forms C═N bonds. The PH- and PEIgPH-containing LiTFSI species are denoted as PHE and HE-PEIgPHE, respectively. Using a practical solution casting method, SSPEs with and without PEI were fabricated (details can be found in the Supporting Information).

As displayed in Figure 1b, the as-prepared PHE membrane is opaque, indicating the existence of a PH crystal or phase separation between PH and LiTFSI. However, the resulting HE-PEIgPHE is transparent and light-yellowish, demonstrating the disorder of the PH crystal and the prevention of Li salt clustering possibly due to a click-like reaction between PH and PEI. The surface morphologies of these SSPEs were investigated by using scanning electron microscopy (SEM). The PHE membrane exhibited a highly porous structure (Figure 1c), implying that the Li^+ conducting pathway is partially disconnected. In sharp contrast, a quite dense structure was observed for HE-PEIgPHE (Figure 1d), suggesting that the polymeric ligand results in a more homogeneous morphology. As investigated in Figure 1e and Figure S1, all of the elements fluoride (F), nitrogen (N), and sulfur (S) are well-distributed in the cross-sectional HE-PEIgPHE and PHE, demonstrating homogeneous mixing of PEI and PH chains. Interestingly, HE-PEIgPHE can be bent, folded, and twisted without any deterioration. Such flexibility is advantageous for assembling flexible SSLMBs (Figure 1f). We varied the weight ratio of PH and PEI to enhance the mechanical properties (Figure S2) and found that the tensile strength reaches a maximum of 11.63 MPa at an optimum PEI content of 15 wt %. While fixing the PH/PEI ratio, we varied the LiTFSI content with respect to the PH and monitored the stress and strain behavior. A maximum tensile strength was achieved at an intermediate PH/LiTFSI weight ratio of 1.5:1 (Figure S3).

To identify the cross-linking click-like reaction, the Fourier transform infrared (FT-IR) spectra were obtained (Figure 1g). The major peaks of dimethylformamide (DMF) are located at 2930, 2859, and around 500–1600 cm^{-1}, but they almost disappeared in the PH, suggesting the complete evaporation of DMF during the drying process. After the introduction of PEI into the PH system, the peaks in HE-PEIgPHE change slightly in comparison with the pure PH curve. A new peak at 1650 cm^{-1} corresponding to the C═N stretch on HE-PEIgPHE indicates the successful cross-linking between PH and PEI molecules. Also, the peak at 1571 cm^{-1} of the N–H stretching vibration on the original PEI molecular chain shifted to 1560 cm^{-1}, further supporting an effective grafting reaction.[18,40]

https://doi.org/10.1021/acs.nanolett.4c00154
Nano Lett. 2024, 24, 6850–6857

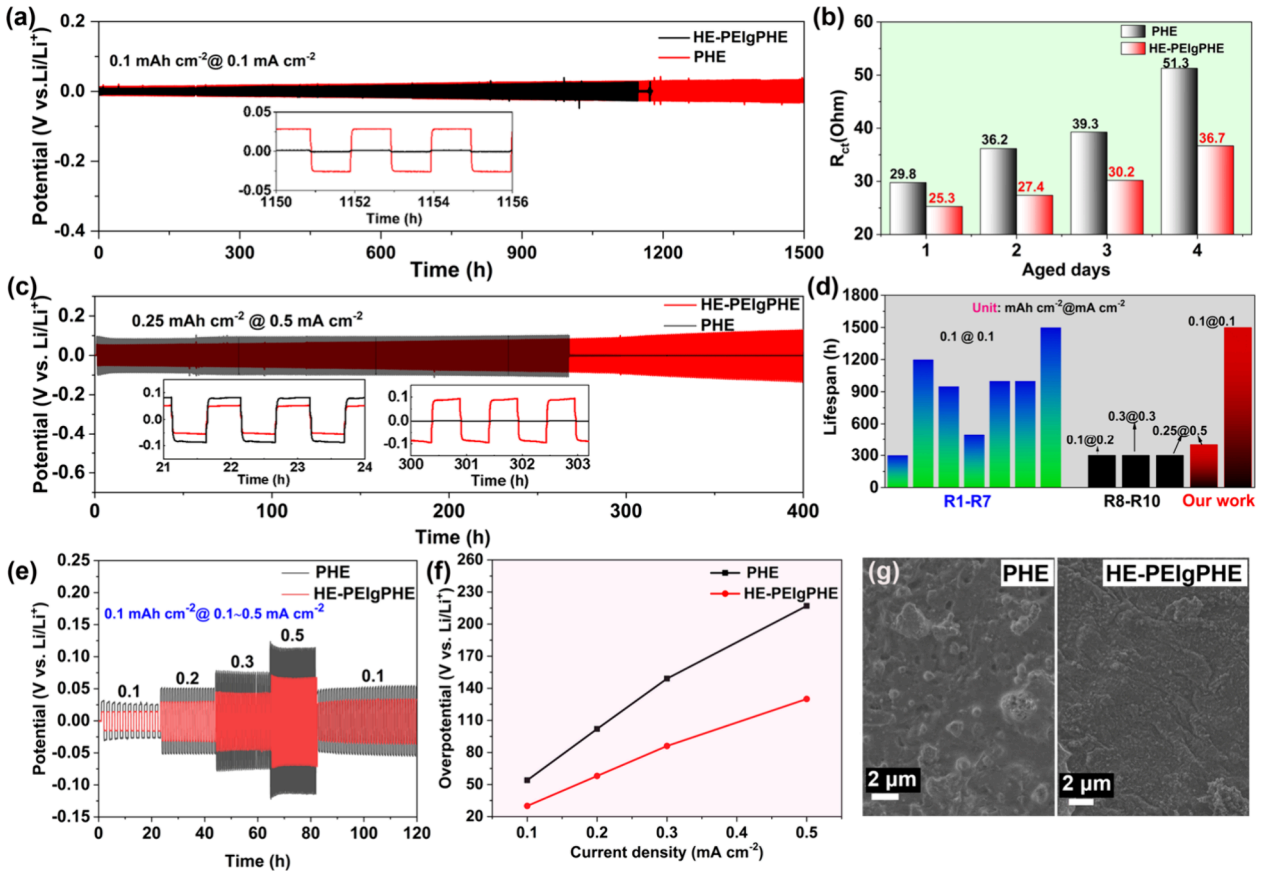

Figure 3. Electrochemical characterization of a Li|Li symmetric cell based on various SSPEs. (a) Voltage−time curves of symmetric cells with HE-PEIgPHE and PHE at 60 °C at 0.1 mA cm^{-2} and an areal capacity density of 0.1 mAh cm^{-2}. (b) Storage time dependence of resistance of Li|HE-PEIgPHE|Li cells at 60 °C. (c) Voltage−time curves of symmetric cells with HE-PEIgPHE and PHE at 60 °C at 0.5 mA cm^{-2} under an areal capacity of 0.25 mAh cm^{-2}. (d) Comparison of other reported works and our HE-PEIgPHE. (e) Voltage−time curves of symmetric cells with HE-PEIgPHE and PHE at various current densities. (f) The overpotential at various test conditions for HE-PEIgPHE and PHE, respectively. (g, h) SEM images of the Li surface for the cycled Li|Li cells with PHE and HE-PEIgPHE, respectively.

Meanwhile, the intensity of peaks observed at 3358 and 3280 cm^{-1} for the NH_2 stretching vibrations of PEI and the peak at 1060 cm^{-1} for the CF_3 stretching vibration of PH became much weaker in the HE-PEIgPHE, demonstrating the effective reaction between $-CF_3$ and $-NH_2$. Furthermore, the XPS spectrum of N 1s (Figure 1h) demonstrates the existence of C═N (398.6 eV), C−N (399.6 eV), and N−H bonds (400.7 eV),[40] solidly supporting the reaction of PH and PEI. Besides, the multivariant network structure of the HE-PEIgPHE derived from the abundant amines is capable of accelerating Li^+ transport near the bridged and disordered skeleton.[42] Successively, the thermal, mechanical, and electrochemical properties of the high-entropy SSPE were comprehensively studied, as shown in Figure 2. Differential scanning calorimetry (DSC) curves for PHE and HE-PEIgPHE membranes were assessed and are shown in Figure 2a, respectively. The comparison of the DSC curves reveals that the melting temperature of a PH crystal in PHE (143 °C) was reduced to 134 °C with the incorporation of the polymeric ligand, which indicates the partial destruction of the PH crystal structure by the grafting reaction.[43,44] It supports that PH chains are in a more disordered state in HE-PEIgPHE, improving Li^+ conductivity. The thermal stability was evaluated for HE-PEIgPHE and PHE using a thermal gravimetric analyzer (TGA) (Figure 2b). As the temperature was increased, HE-PEIgPHE and PHE both exhibited slight weight loss from the evaporation of residual DMF solvent and great weight loss because of the decomposition of electrolytes. The higher decomposition temperature (343 °C) for HE-PEIgPHE than for PHE (310 °C) suggests a practical reaction of PEI and PH. The incorporation of PEI increases the tensile strength from 5.18 (PHE) to 6.78 MPa (HE-PEIgPHE) and decreases the elongation break from 272% (PHE) to 170% (HE-PEIgPHE) (Figure S4), which supports successful multivariant grafting in HE-PEIgPHE. The increase in Young's modulus can be beneficial in inhibiting the growth of Li dendrites when used for SSLMBs.

To investigate the effect of the structural disorder on Li^+ transport, stainless steel (SS)|HE-PEIgPHE (or PHE)|SS symmetric cells were assembled and the ionic conductivities of HE-PEIgPHE and PHE were quantified using impedance analysis at different temperatures (Figure 2c and Figure S5). As expected, the ionic conductivities are higher for HE-PEIgPHE regardless of the temperature. The ionic conductivity at 60 °C of HE-PEIgPHE (2.14×10^{-4} S cm^{-1}) is above 2 times higher than that of PHE (1.03×10^{-4} S cm^{-1}). This improvement can be ascribed to the following aspects: (1) PH grafting provides a structural disorder in the crystal structure of PH and reduces the crystallinity; (2) It facilitates Li^+ transport along the disordered polymer matrix and inhibits the movement of $TFSI^-$ due to the unreacted NH_2 groups in PEI. Meanwhile, the slope of the Arrhenius curve, which corresponds to the

https://doi.org/10.1021/acs.nanolett.4c00154
Nano Lett. 2024, 24, 6850−6857

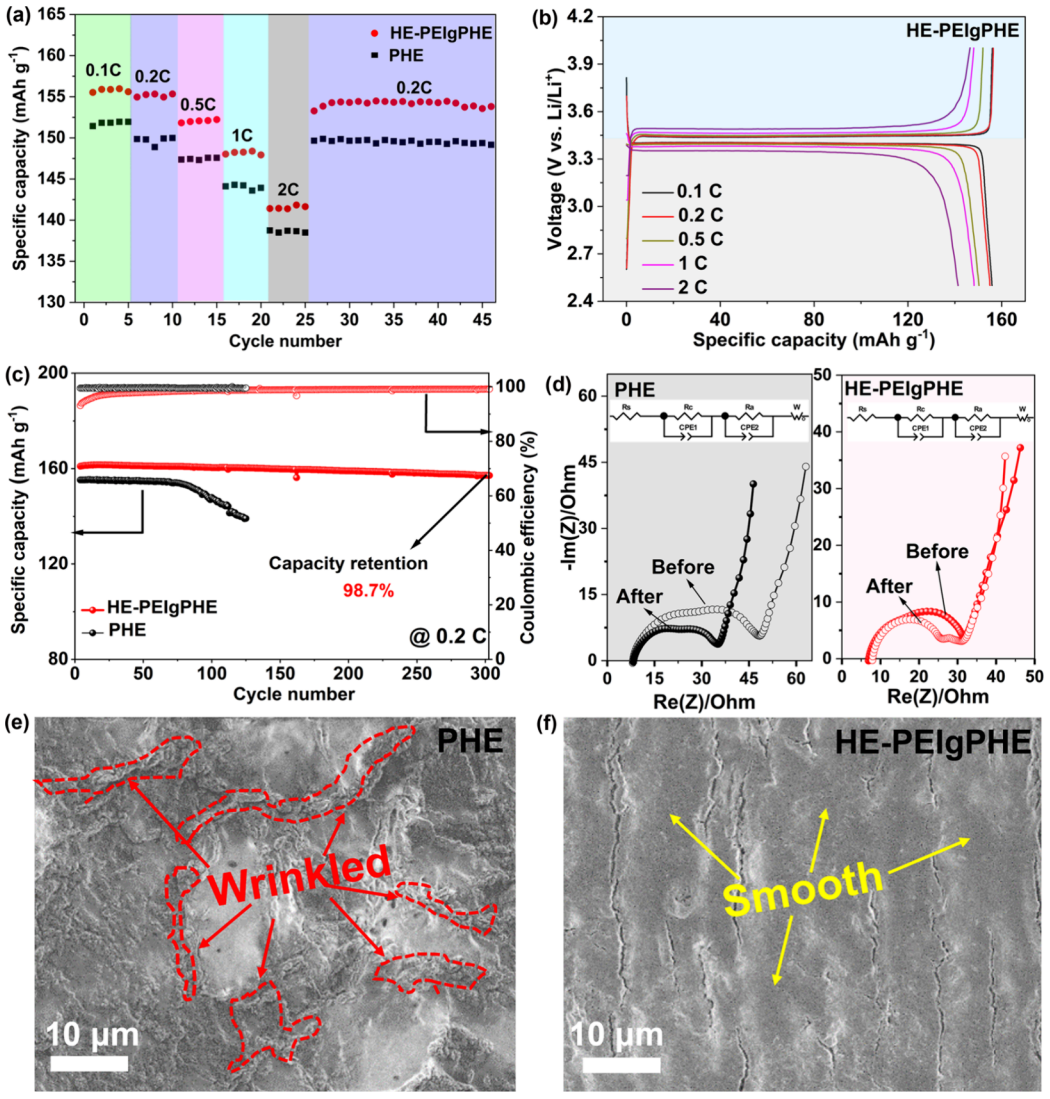

Figure 4. Characterization of Li|PHE|$LiFePO_4$ and Li|PHE|$LiFePO_4$ full cells at 60 °C. (a) Rate performance. (b) Voltage profiles of the Li|HE-PEIgPHE|$LiFePO_4$ cell at different charging/discharging rates. (c). Long cycling performance at 0.2 C. (d) The equivalent circuit (inset) and EIS curves before and after 100 cycles. (e, f) Surface morphologies of cycled Li metal at 0.2 C for 100 cycles.

activation energy (E_a) for ionic conduction, was lower for HE-PEIgPHE (20.22 kJ mol^{-1}) compared with that for PHE (25.04 kJ mol^{-1}), indicating facilitated Li^+ transport in HE-PEIgPHE. Furthermore, the Li^+ transference number was also evaluated for the two SSPEs at a constant temperature of 60 °C (Figure 2e). According to the constant-current polarization curves (Figure S6a,b) and the calculation formula, the Li^+ transference numbers of HE-PEIgPHE and PHE are estimated to be 0.55 and 0.42, respectively. The increase in Li^+ transference number is probably due to the facilitated Li^+ transport along the disordered polymer matrix and/or inhabited movement of $TFSI^-$ due to its interaction with unreacted NH_2 groups.[32,41] The high Li^+ transference number can alleviate the electrode polarization at the Li metal interface and contribute to achieve uniform Li deposition. To reveal the potential application of HE-PEIgPHE in high-energy-density SSLMBs, the electrochemical stability window of HE-PEIgPHE was examined (Figure 2f). As shown, HE-PEIgPHE has a higher voltage window (4.5 V vs Li/Li^+) than that of PHE (4.0 V vs Li/Li^+), indicating that HE-PEIgPHE has good electrochemical stability for batteries at higher voltages. This is in agreement with the inhibited transport of $TFSI^-$ that is prone to anodic decomposition at high voltages.

In order to evaluate the interfacial stability and compatibility of HE-PEIgPHE with a Li metal anode, Li plating/stripping tests were performed with Li/HE-PEIgPHE/Li symmetric cells (Figure 3). As shown in Figure 3a, our designed high-entropy SSPE enables the Li|HE-PEIgPHE|Li symmetric cell to last for more than 1500 h and possess a low polarization voltage of 30 mV at 0.1 mA cm^{-2}, which are much longer than those of a control Li|PHE|Li cell having a short circuit after cycling for 1150 h, indicating that the solid electrolyte interface (SEI) film formed in the HE-PEIgPHE-based cell is more stable and has a better compatibility with the Li metal anode. Furthermore, the aging of interface stability of HE-PEIgPHE was also evaluated by electrochemical impedance spectroscopy (EIS) at 60 °C for 4 days (Figure 3b and Figure S7). The initial interface resistance for HE-PEIgPHE was 29.8 Ω after 1 day of storage and then increased to 36.2, 39.3, and 51.3 Ω after aging for 2, 3, and 4 days, respectively. These values are much larger than the corresponding values of HE-PEIgPHE, indicating an improved interface compatibility with HE-PEIgPHE. Even

https://doi.org/10.1021/acs.nanolett.4c00154
Nano Lett. 2024, 24, 6850−6857

under harsher operating conditions (current density of 0.5 mA cm^{-2} and plating capacity of 0.25 mAh cm^{-2}), the overpotential for HE-PEIgPHE was maintained below 100 mV over 300 h (Figure 3c). Compared with some previously reported SSPE-based Li|Li cells (Figure 3d and Table S1), HE-PEIgPHE exhibits an impressive and outstanding cycling lifespan or plating current density. The rate performance of the Li|Li symmetric cell for the high-entropy HE-PEIgPHE also verifies its interface stability at high current densities (Figure 3e). As observed, the cell voltages under Li plating/stripping were extraordinarily stable for HE-PEIgPHE even with an increase of current density from 0.1 to 0.5 mA cm^{-2}, and the cell polarizations of HE-PEIgPHE were obviously smaller than those of PHE (Figure 3f), indicating that the high-entropy design is beneficial for improving the interface stability with the multivariant grafting of PH. After cycling, the SEI structure and the morphology of cycled Li metal are subjected to SEM and XPS measurements. Compared with PHE (Figure 3g), HE-PEIgPHE showed a more homogeneous Li morphology (Figure 3h), in good agreement with the electrochemical analysis. From the XPS spectra of C 1s and F 1s on the surface of Li metal (Figure S8), LiF, $TFSI^-$, Li_2CO_3, and organic compounds were identified. These products could be attributed to the decomposition of Li salts and the PH matrix. However, a comparison of the F 1s spectra for PHE and HE-PEIgPHE (Figure S8b,d) reveals that the LiF content is lower for HE-PEIgPHE. This suggests that the decomposition of PHE and/or $TFSI^-$ at the Li surface was suppressed with HE-PEIgPHE, which agrees with the lower transport of $TFSI^-$ in HE-PEIgPHE. Also, the high-resolution XPS spectrum of N 1s for HE-PEIgPHE was collected and exhibited in Figure S9, and a fitted peak at about 396 eV for an N−Li bond is observed and ascribed to the formation of Li_3N resulting from the electrochemical reaction between negligible unreacted $-NH_2$ and Li metal, exhibiting a tight contact between the SSPE and metallic Li.

Furthermore, HE-PEIgPHE and PHE fabricated Li|SSPEs|$LiFePO_4$ SSLMBs were used to evaluate the potential application of our high-entropy SSPEs (Figure 4). Their rate performances from 0.1 to 2 C (Figure 4a) show that the discharge specific capacities for Li|HE-PEIgPHE|$LiFePO_4$ are 155.6, 155.1, 152.0, 148.1, and 141.5 mAh g^{-1} at 0.1, 0.2, 0.5, 1, and 2 C (1 C=170 mA g^{-1}), respectively, which are much larger than those of the Li|PHE|$LiFePO_4$ cell at the same current density. Especially, when the current density returned to 0.2 C, the Li|HE-PEIgPHE|$LiFePO_4$ cell could recover its capacity at 154 mAh g^{-1}. Also, a slightly lower voltage polarization for HE-PEIgPHE (Figure 4b) than that for PHE (Figure S10) further supports the idea that HE-PEIgPHE displays a better compatibility with electrodes and excellent electrochemical reversibility in SSLMBs. Their cycling performance at 0.2 C obviously verify that, compared with Li|PHE|$LiFePO_4$ cells, the Li|HE-PEIgPHE|$LiFePO_4$ cell delivers a higher initial specific capacity (162 vs 155 mAh g^{-1}), a longer lifetime (300 vs 125 cycles), and an excellent capacity retention of 98.7% (Figure 4c). To further determine the origin of HE-PEIgPHE in improving the electrochemical performance of SSLMBs, the EIS and surface morphologies of Li metal before and after cycling were collected (Figure 4d−f). As shown, in comparison to the Li|PHE|$LiFePO_4$ cell with a large increase in the exchange resistance, the Li|HE-PEIgPHE|$LiFePO_4$ cell is relatively stable (Table S2 and Figure 4d), indicating a better and more stable interface of HE-PEIgPHE in SSLMBs. Also, a mossy and wrinkled surface for Li metal from the PHE-based cell (Figure 4e) and a relatively smooth surface for Li metal from the HE-PEIgPHE cell (Figure 4f) was observed, indicating that our HE-PEIgPHE could guide the uniform deposition of Li^+ and form a more stable SEI film. To explore the application of HE-PEIgPHE in high-voltage cathodes, Li|HE-PEIgPHE|$Li(Ni_{0.5}Co_{0.2}Mn_{0.3})O_2$ (NCM523) full cells were assembled and tested. As shown in Figure S11, it was found that the cell can be charged to 4.3 V normally, and the initial discharge specific capacity was 156 mAh g^{-1} at 0.1C. After the initial activation, a reversible specific capacity of 150 mAh g^{-1} at 0.2 C and a CE of 91% can be realized, suggesting that our HE-PEIgPHE can match with the NCM523 cathode. As summarized in Table S3, it is obvious that the performance of high-entropy SSPE is comparable to that of other strategies of mixing a polymer with inorganic particles, improving ionic conductivity and decreasing interface resistance. Therefore, our HE-PEIgPHE has a great future in constructing high-performance SSLMBs.

In summary, we have successfully developed a novel high-entropy HE-PEIgPHE SSPE by multivalent grafting of PH on PEI polymeric ligands via a multidirectional click-like reaction. The HE-PEIgPHE exhibits a high Young's modulus (6.78 MPa), high ionic conductivity (2.14×10^{-4} S cm^{-1}), high Li^+ transference number (0.55), and wide electrochemical stability window (4.5 V) due to the structural disorder caused by the multivalent grafting. Our high-entropy HE-PEIgPHE expectedly boosts the electrochemical performance of SSLMBs, e.g., a high reversible specific capacity of up to 160 mAh g^{-1} at 0.2 C and a long lifetime of 1500 h at 0.1 mA cm^{-2}, demonstrating an effective route to develop high-entropy SSPEs by multivariant grafting of polymers to advance the performance of SSLMBs.

■ ASSOCIATED CONTENT

Supporting Information

The Supporting Information is available free of charge at https://pubs.acs.org/doi/10.1021/acs.nanolett.4c00154.

Experimental section and some supporting data, such as SEM, *i*−*t* profile, EIS, and XPS (PDF)

■ AUTHOR INFORMATION

Corresponding Authors

Fangmin Ye − *Key Laboratory of Optical Field Manipulation of Zhejiang Province, Department of Physics, Zhejiang Sci-Tech University, Hangzhou 310018, People's Republic of China;* orcid.org/0000-0001-6595-0881; Email: fmye2013@sinano.ac.cn

Aiping Liu − *Key Laboratory of Optical Field Manipulation of Zhejiang Province, Department of Physics, Zhejiang Sci-Tech University, Hangzhou 310018, People's Republic of China;* orcid.org/0000-0002-2338-062X; Email: liuaiping1979@gmail.com

Hee-Tak Kim − *Department of Chemical and Biomolecular Engineering, Korea Advanced Institute of Science and Technology (KAIST), Daejeon 34141, Republic of Korea;* orcid.org/0000-0003-4578-5422; Email: heetak.kim@kaist.ac.kr

Jian Wang − *i-Lab & CAS Key Laboratory of Nanophotonic Materials and Devices, Suzhou Institute of Nano-Tech and Nano-Bionics, Chinese Academy of Sciences, Suzhou 215123, People's Republic of China; Helmholtz Institute Ulm (HIU),*

https://doi.org/10.1021/acs.nanolett.4c00154
Nano Lett. 2024, 24, 6850−6857

Ulm D89081, Germany; Karlsruhe Institute of Technology (KIT), D76021 Karlsruhe, Germany; Email: jian.wang@kit.edu, wangjian2014@sinano.ac.cn

Authors

Zhixin Wang − *Key Laboratory of Optical Field Manipulation of Zhejiang Province, Department of Physics, Zhejiang Sci-Tech University, Hangzhou 310018, People's Republic of China*

Mengcheng Li − *Key Laboratory of Optical Field Manipulation of Zhejiang Province, Department of Physics, Zhejiang Sci-Tech University, Hangzhou 310018, People's Republic of China*

Jing Zhang − *School of Materials Science and Engineering, Xi'an University of Technology, Xi'an 710048, People's Republic of China*

Dong Wang − *Key Laboratory of Automobile Materials of MOE, School of Materials Science and Engineering, Jilin University, Changchun 130012, People's Republic of China*; orcid.org/0000-0003-2456-6175

Meinan Liu − *i-Lab & CAS Key Laboratory of Nanophotonic Materials and Devices, Suzhou Institute of Nano-Tech and Nano-Bionics, Chinese Academy of Sciences, Suzhou 215123, People's Republic of China*; orcid.org/0000-0003-2552-1091

Hongzhen Lin − *i-Lab & CAS Key Laboratory of Nanophotonic Materials and Devices, Suzhou Institute of Nano-Tech and Nano-Bionics, Chinese Academy of Sciences, Suzhou 215123, People's Republic of China*

Complete contact information is available at: https://pubs.acs.org/10.1021/acs.nanolett.4c00154

Author Contributions

○F.Y., Z.W., and M.L. contributed equally to this work.

Notes

The authors declare no competing financial interest.

■ ACKNOWLEDGMENTS

This work was supported by the National Key R&D Program of China (2021YFA1201503), the National Natural Science Foundation of China (Nos. 22075313; 22309144; 21972164; 22279161; 11734013), the Science Foundation of Zhejiang Sci-Tech University (18062299-Y), the Natural Science Foundation of Jiangsu Province (BK. 20210130), and Innovative and Entrepreneurial Doctor in Jiangsu Province (JSSCBS20211428). J.W. acknowledges the funding support provided by the Alexander von Humboldt Foundation and the basic funding of the Helmholtz Association. The author also acknowledges the support from Nano-X, Suzhou Institute of Nanotech and Nanobionics, Chinese Academy of Sciences.

■ REFERENCES

(1) Garcia-Barriocanal, J.; Rivera-Calzada, A.; Varela, M.; Sefrioui, Z.; Iborra, E.; Leon, C.; Pennycook, S. J.; Santamaria, J. Colossal ionic conductivity at interfaces of epitaxial ZrO_2: Y_2O_3/$SrTiO_3$ heterostructures. *Science* **2008**, *321*, 676−680.

(2) Wu, Q.; Zheng, Y.; Guan, X.; Xu, J.; Cao, F.; Li, C. Dynamical SEI Reinforced by Open-Architecture MOF Film with Stereoscopic Lithiophilic Sites for High-Performance Lithium−Metal Batteries. *Adv. Funct. Mater.* **2021**, *31*, 2101034.

(3) Wang, J.; Hu, H.; Duan, S.; Xiao, Q.; Zhang, J.; Liu, H.; Kang, Q.; Jia, L.; Yang, J.; Xu, W.; Fei, H.; Cheng, S.; Li, L.; Liu, M.; Lin, H.; Zhang, Y. Construction of Moisture-Stable Lithium Diffusion-Controlling Layer toward High Performance Dendrite-Free Lithium. *Anode. Adv. Funct. Mater.* **2022**, *32*, 2110468.

(4) Yao, Y. L.; Zhu, M. Y.; Zhao, Z.; Tong, B. H.; Fan, Y. Q.; Hua, Z. S. Hydrometallurgical Processes for Recycling Spent Li-Ion Batteries: A Critical Review., *ACS Sustain. Chem. Eng.* **2018**, *6*, 13611−13627.

(5) Li, J. L.; Fleetwood, J.; Hawley, W. B.; Kays, W. From Materials to Cell: State-of-the-Art and Prospective Technologies for Li-Ion Battery Electrode Processing. *Chem. Rev.* **2022**, *122*, 903−956.

(6) Zhao, Y. L.; Yuan, X. Z.; Jiang, L. B.; Wen, J.; Wang, H.; Guan, R. P.; Zhang, J. J.; Zeng, G. M. Regeneration and reutilization of cathode materials from spent Li-ion batteries. *Chem. Eng. J.* **2020**, *383*, 123089.

(7) Wang, Q. S.; Ping, P.; Zhao, X. J.; Chu, G. Q.; Sun, J. H.; Chen, C. H. Thermal runaway caused fire and explosion of Li ion battery. *J. Power Sources* **2012**, *208*, 210−224.

(8) Ruiz, V.; Pfrang, A.; Kriston, A.; Omar, N.; Van den Bossche, P.; Boon-Brett, L. A review of international abuse testing standards and regulations for Li ion batteries in electric and hybrid electric vehicles. *Renew. Sust. Energy Rev.* **2018**, *81*, 1427−1452.

(9) Zhang, J.; You, C.; Lin, H.; Wang, J. Electrochemical Kinetic Modulators in Lithium−Sulfur Batteries: From Defect-Rich Catalysts to Single Atomic Catalysts. *Energy Environ. Mater.* **2022**, *5*, 731−750.

(10) Wang, J.; Zhang, J.; Duan, S.; Jia, L.; Xiao, Q.; Liu, H.; Hu, H.; Cheng, S.; Zhang, Z.; Li, L.; Duan, W.; Zhang, Y.; Lin, H. Lithium Atom Surface Diffusion and Delocalized Deposition Propelled by Atomic Metal Catalyst toward Ultrahigh-Capacity Dendrite-Free Lithium Anode. *Nano Lett.* **2022**, *22*, 8008−8017.

(11) Wang, J.; Li, L.; Hu, H.; Hu, H.; Guan, Q.; Huang, M.; Jia, L.; Adenusi, H.; Tian, K. V.; Zhang, J.; Passerini, S.; Lin, H. Toward Dendrite-Free Metallic Lithium Anodes: From Structural Design to Optimal Electrochemical Diffusion Kinetics. *ACS Nano* **2022**, *16*, 17729−17760.

(12) Wang, J.; Zhang, J.; Wu, J.; Huang, M.; Jia, L.; Li, L.; Zhang, Y.; Hu, H.; Liu, F.; Guan, Q.; Liu, M.; Adenusi, H.; Lin, H.; Passerini, S. Interfacial "Single-Atom-in-Defects" Catalysts Accelerating Li^+ Desolvation Kinetics for Long-Lifespan Lithium-Metal Batteries. *Adv. Mater.* **2023**, *35*, 2302828.

(13) Wang, J.; Jia, L. J.; Zhong, J.; Xiao, Q. B.; Wang, C.; Zang, K. T.; Lin, H. T.; Zheng, H. C.; Luo, J.; Yang; Fan, H. Y.; Duan, W. H.; Wu, Y.; Lin, H. Z.; Zhang, Y. G. Single-atom catalyst boosts electrochemical conversion reactions in batteries. *Energy Storage Mater.* **2019**, *18*, 246−252.

(14) Francis, C. F. J.; Kyratzis, I. L.; Best, A. S. Li-Ion Battery Separators for Ionic-Liquid Electrolytes: A Review. *Adv. Mater.* **2020**, *32*, 1904205.

(15) Manthiram, A. An Outlook on Li Ion Battery Technology. *ACS Central Sci.* **2017**, *3*, 1063−1069.

(16) Wang, Y.; Zhong, W. H. Development of Electrolytes towards Achieving Safe and High-Performance Energy-Storage Devices A Review. *Chemelectrochem* **2015**, *2*, 22−36.

(17) Tan, S. J.; Zeng, X. X.; Ma, Q.; Wu, X. W.; Guo, Y. G. Recent Advancements in Polymer-Based Composite Electrolytes for Rechargeable Li Batteries. *Electrochem. Energy Rev.* **2018**, *1*, 113−138.

(18) Wan, J. Y.; Xie, J.; Kong, X.; Liu, Z.; Liu, K.; Shi, F. F.; Pei, A.; Chen, H.; Chen, W.; Chen, J.; Zhang, X. K.; Zong, L. Q.; Wang, J. Y.; Chen, L. Q.; Qin, J.; Cui, Y. Ultrathin, flexible, solid polymer composite electrolyte enabled with aligned nanoporous host for Li batteries. *Nat. Nanotechnol.* **2019**, *14*, 705.

(19) Dong, H. B.; Li, J. W.; Guo, J.; Lai, F. L.; Zhao, F. J.; Jiao, Y. D.; Brett, D. J. L.; Liu, T. X.; He, G. J.; Parkin, I. P. Insights on Flexible Zinc-Ion Batteries from Lab Research to Commercialization. *Adv. Mater.* **2021**, *33*, 2007548.

(20) Wu, Z. J.; Xie, Z. K.; Yoshida, A.; Wang, Z. D.; Hao, X. G.; Abudula, A.; Guan, G. Q. Utmost limits of various solid electrolytes in all-solid-state Li batteries: A critical review. *Renew. Sust. Energy Rev.* **2019**, *109*, 367−385.

(21) Yu, X. W.; Manthiram, A. A review of composite polymer-ceramic electrolytes for Li batteries. *Energy Storage Mater.* **2021**, *34*, 282−300.

(22) Wang, X.; Zhai, H. W.; Qie, B. Y.; Cheng, Q.; Li, A. J.; Borovilas, J.; Xu, B. Q.; Shi, C. M.; Jin, T. W.; Liao, X. B.; Li, Y. B.; He, X. D.; Du, S. Y.; Fu, Y. K.; Dontigny, M.; Zaghib, K.; Yang, Y. Rechargeable solid-state Li metal batteries with vertically aligned ceramic nanoparticle/polymer composite electrolyte. *Nano Energy* **2019**, *60*, 205−212.
(23) Fan, L. Z.; He, H. C.; Nan, C. W. Tailoring inorganic-polymer composites for the mass production of solid-state batteries. *Nat. Rev. Mater.* **2021**, *6*, 1003−1019.
(24) Bae, J.; Li, Y. T.; Zhang, J.; Zhou, X. Y.; Zhao, F.; Shi, Y.; Goodenough, J. B.; Yu, G. H. A 3D Nanostructured Hydrogel-Framework-Derived High-Performance Composite Polymer Li-Ion Electrolyte. *Angew. Chem., Int. Ed.* **2018**, *57*, 2096−2100.
(25) Chen, R. J.; Qu, W. J.; Guo, X.; Li, L.; Wu, F. The pursuit of solid-state electrolytes for Li batteries: from comprehensive insight to emerging horizons. *Mater. Horiz.* **2016**, *3*, 487−516.
(26) Zhang, J. J.; Zhao, J. H.; Yue, L. P.; Wang, Q. F.; Chai, J. C.; Liu, Z. H.; Zhou, X. H.; Li, H.; Guo, Y. G.; Cui, G. L.; Chen, L. Q. Safety-Reinforced Poly(Propylene Carbonate)-Based All-Solid-State Polymer Electrolyte for Ambient-Temperature Solid Polymer Li Batteries. *Adv. Energy Mater.* **2015**, *5*, 1501082.
(27) Zhao, Q.; Liu, X. T.; Stalin, S.; Khan, K.; Archer, L. A. Solid-state polymer electrolytes with in-built fast interfacial transport for secondary Li batteries. *Nat. Energy* **2019**, *4*, 365−373.
(28) Wu, K.; Huang, J. H.; Yi, J.; Liu, X. Y.; Liu, Y. Y.; Wang, Y. G.; Zhang, J. J.; Xia, Y. Y. Recent Advances in Polymer Electrolytes for Zinc Ion Batteries: Mechanisms, Properties, and Perspectives. *Adv. Energy Mater.* **2020**, *10*, 1903977.
(29) Liu, W.; Liu, N.; Sun, J.; Hsu, P. C.; Li, Y. Z.; Lee, H. W.; Cui, Y. Ionic Conductivity Enhancement of Polymer Electrolytes with Ceramic Nanowire Fillers. *Nano Lett.* **2015**, *15*, 2740−2745.
(30) Fares, R. L.; Webber, M. E. What are the tradeoffs between battery energy storage cycle life and calendar life in the energy arbitrage application? *J. Energy Storage* **2018**, *16*, 37−45.
(31) Chen, L.; Li, Y. T.; Li, S. P.; Fan, L. Z.; Nan, C. W.; Goodenough, J. B. PEO/garnet composite electrolytes for solid-state Li batteries: From ″ceramic-in-polymer″ to ″polymer-in-ceramic″. *Nano Energy* **2018**, *46*, 176−184.
(32) Zhao, Y.; Huang, Z.; Chen, S.; Chen, B.; Yang, J.; Zhang, Q.; Ding, F.; Chen, Y.; Xu, X. A promising PEO/LAGP hybrid electrolyte prepared by a simple method for all-solid-state lithium batteries. *Solid State Ionics* **2016**, *295*, 65−71.
(33) Fu, J.; Xu, Y.; Dong, L.; Chen, L.; Lu, Q.; Li, M.; Zeng, X.; Dai, S.; Chen, G.; Shi, L. Multiclaw-shaped octasilsesquioxanes functionalized ionic liquids toward organic-inorganic composite electrolytes for lithium-ion batteries. *Chem. Eng. J.* **2021**, *405*, 126942.
(34) Nie, L.; Gao, R.; Zhang, M.; Zhu, Y.; Wu, X.; Lao, Z.; Zhou, G. Integration of porous high-loading electrode and gel polymer electrolyte for high-performance quasi-solid-state battery. *Adv. Energy Mater.* **2024**, *14*, 2302476.
(35) Wen, S. J.; Luo, C.; Wang, Q. R.; Wei, Z. Y.; Zeng, Y. X.; Jiang, Y. D.; Zhang, G. Z.; Xu, H. L.; Wang, J.; Wang, C. Y.; Chang, J.; Deng, Y. H. Integrated design of ultrathin tcrosslinked network polymer electrolytes for flexible and stable all-solid-state Li batteries. *Energy Storage Mater.* **2022**, *47*, 453−461.
(36) Dong, L. N.; Zeng, X. F.; Fu, J. F.; Chen, L. Y.; Zhou, J.; Dai, S. W.; Shi, L. Y. Cross-linked ionic copolymer solid electrolytes with loose Coordination-assisted Li transport for Li batteries. *Chem. Eng. J.* **2021**, *423*, 130209.
(37) Su, Y.; Rong, X.; Li, H.; Huang, X.; Chen, L.; Liu, B.; Hu, Y. High-Entropy Microdomain Interlocking Polymer Electrolytes for Advanced All-Solid-State Battery Chemistries. *Adv. Mater.* **2023**, *35*, 2209402.
(38) Kim, S. C.; Wang, J.; Xu, R.; Zhang, P.; Chen, Y.; Huang, Z.; Yang, Y.; Yu, Z.; Oyakhire, S.; Zhang, W.; Greenburg, L. C.; Kim, M. S.; Boyle, D. T.; Sayavong, P.; Ye, Y.; Qin, J.; Bao, Z.; Cui, Y. High-entropy electrolytes for practical lithium metal batteries. *Nat. Energy* **2023**, *8*, 814.
(39) Liu, W. Y.; Yi, C. J.; Li, L. P.; Liu, S. L.; Gui, Q. Y.; Ba, D. L.; Li, Y. Y.; Peng, D. L.; Liu, J. P. Designing Polymer-in-Salt Electrolyte and Fully Infiltrated 3D Electrode for Integrated Solid-State Li Batteries. *Angew. Chem., Int. Ed.* **2021**, *60*, 12931−12940.
(40) Liu, H.; Zhou, Y.; Yang, Y.; Zou, K.; Wu, R.; Xia, K.; Xie, S. Synthesis of polyethylenimine/graphene oxide for the adsorption of U(VI) from aqueous solution. *Appl. Surf. Sci.* **2019**, *471*, 88−95.
(41) Zhou, Y.; Zhang, L.; Huang, W.; Kong, Q.; Fan, X.; Wang, M.; Shi, J. N-doped graphitic carbon-incorporated g-C_3N_4 for remarkably enhanced photocatalytic H2 evolution under visible light. *Carbon* **2016**, *99*, 111−117.
(42) Zhang, J. X.; Zhu, C. Q.; Xu, J.; Wu, J.; Yin, X. Z.; Chen, S. H.; Zhu, Z. M.; Wang, L. X.; Li, Z. C. Enhanced mechanical behavior and electrochemical performance of composite separator by constructing crosslinked polymer electrolyte networks on polyphenylene sulfide nonwoven surface. *J. Membr. Sci.* **2020**, *597*, No. 117622.
(43) Wang, X. Y.; Xiao, C. F.; Liu, H. L.; Chen, M. X.; Xu, H. Y.; Luo, W. P.; Zhang, F. Robust functionalization of underwater superoleophobic PH tubular nanofiber membranes and applications for continuous dye degradation and oil/water separation. *J. Membr. Sci.* **2020**, *596*, 117583.
(44) Zhou, R.; Liu, W. S.; Kong, J. H.; Zhou, D.; Ding, G. Q.; Leong, Y. W.; Pallathadka, P. K.; Lu, X. H. Chemically cross-linked ultrathin electrospun poly(vinylidene fluoride-co-hexafluoropropylene) nanofibrous mats as ionic liquid host in electrochromic devices. *Polymer* **2014**, *55*, 1520−1526.

https://doi.org/10.1021/acs.nanolett.4c00154
Nano Lett. 2024, 24, 6850−6857